The Astrophysical Journal, 638:1154–1161, 2006 February 20

Si XII X-RAY SATELLITE LINES IN SOLAR FLARE SPECTRA

K. J. H. Phillips
National Research Council Senior Research Associate, NASA Goddard Space Flight Center, Greenbelt, MD 20771;
kennethjhphillips@yahoo.com

J. Dubau
Observatoire de Paris, LUTH, 92190 Meudon; and Université Paris-Sud, LIXAM, 91405 Orsay, France

and

J. Sylwester and B. Sylwester
Space Research Centre, Polish Academy of Sciences, 51-622, Kopernika 11, Wrocław, Poland
Received 2005 August 23; accepted 2005 October 23

ABSTRACT

The temperature dependence of the Si XII $n = 3$ and 4 dielectronic satellite line features at 5.82 and 5.56 Å, respectively, near the Si XIII $1s^2$–$1s3p$ and $1s^2$–$1s4p$ lines (5.681 and 5.405 Å), is calculated using atomic data presented here. The resulting theoretical spectra are compared with solar flare spectra observed by the RESIK spectrometer on the *CORONAS-F* spacecraft. The satellites, like the more familiar $n = 2$ satellites near the Si XIII $1s^2$–$1s2p$ lines, are formed mostly by dielectronic recombination, but unlike the $n = 2$ satellites, are unblended. The implications for similar satellite lines in flare Fe spectra are discussed.

Subject headings: line: identification — Sun: flares — Sun: X-rays, gamma rays

Online material: color figures

1. INTRODUCTION

A common means of determining the electron temperature T_e of solar active region and flare plasmas is the measurement of intensity ratios I_s/I_w of dielectronic satellite lines emitted by Li-like ions to resonance lines w (transition $1s^2\ ^1S_0$–$1s2p\ ^1P_1$) of He-like ions of, particularly, S, Ca, and Fe, all in the soft X-ray region (wavelengths 1.85–5.03 Å). The satellites are on the long-wavelength side of the w line and have transitions such as $1s^2nl$–$1s2p\ nl$, the electron represented by nl being a nonparticipating (or "spectator") electron. For active region or flare densities ($N_e = 10^{10}$–10^{12} cm^{-3}), satellites in the $1s^2$–$1s2p^2$ array are formed purely by dielectronic recombination of the He-like ion and have intensity ratios with the w line, I_s/I_w, that vary with T_e approximately as T_e^{-1} (Gabriel 1972). Satellites in the $1s^22s$–$1s2s2p$ array [the most intense being q, $1s^22s\ ^2S_{1/2}$–$1s2p\ (^3P)\ 2s\ ^2P_{3/2}$] may also be formed by inner-shell excitation of the Li-like ion. Their intensity ratios I_s'/I_w enable the ratio of Li-like ions and He-like ions to be determined. Although widely used for determining T_e, the I_s/I_w ratios have the disadvantage that the most intense, j and k (transitions $1s^22p\ ^2P_{1/2}$–$1s2p^2\ ^2D_{3/2}$ and $1s^22p\ ^2P_{3/2}$–$1s2p^2\ ^2D_{5/2}$, respectively), are partly or completely blended with the $1s^2\ ^1S_0$–$1s2s\ ^3S_1$ (z or "forbidden") line in a range of He-like ion spectra, including Si.

Feldman et al. (1974), Boiko et al. (1978), and Audebert et al. (1985) obtained X-ray spectra of He-like ions of Si and other elements emitted by high-density ($\sim 10^{21}$ cm^{-3}) laser-produced plasmas. The Si spectra include the $1s^2\ ^1S_0$–$1s3p\ ^1P_1$ line (sometimes referred to as Heβ and called here w_3; wavelength 5.681 Å), blended with a much weaker intercombination, or y_3, line ($1s^2\ ^1S_0$–$1s3p\ ^3P_1$) at 5.689 Å, intensity about 1%–2% of the w_3 line, together with Li-like ion dielectronic satellites having transitions $1s^22l$–$1s2l3l'$ ($l = s$ or p; $l' = s, p$, or d) on the long-wavelength side of, and well separated from, the w_3-y_3 line blend. Although there are many such satellites, the group is dominated by a single line feature at about 5.82 Å. These satellites have also been observed in solar spectra with high-resolution crystal spectrometers (Neupert 1971; Walker & Rugge 1971; Doschek 1972).

Recent solar flare spectra have been obtained with the Rentgenowsky Spektrometr s Izognutymi Kristalami (RESIK) instrument on the Russian *CORONAS-F* mission, launched on 2001 July 31. The instrument, described in detail by Sylwester et al. (2005), is an uncollimated bent crystal spectrometer with four channels covering the wavelength range 3.4–6.1 Å. The instrument's effective areas, derived from a careful assessment of calibration factors, are accurate to better than 20% (Sylwester et al. 2005). Channel 4 of RESIK (range 4.96–6.09 Å for an on-axis source) includes the Si XIII w_3 line (5.681 Å) and the Si XII satellite ($1s^22l$–$1s2l3l'$) feature at 5.82 Å, which are prominent in flare spectra. In addition, the Heγ (called here w_4; transition $1s^2\ ^1S_0$–$1s4p\ ^1P_1$) line at 5.405 Å and the Heδ (w_5; $1s^2\ ^1S_0$–$1s5p\ ^1P_1$) line at 5.286 Å are generally evident, together with line features that we ascribe to Si XII dielectronic satellites with transitions $1s^22l$–$1s2l4l'$ (5.56 Å) and $1s^22l$–$1s2l5l'$ (5.45 Å) (Sylwester et al. 2003). The position of the Si XIII $1s^2\ ^1S_0$–$1s6p\ ^1P_1$ (w_6) line coincides with the Si XIV Lyβ line doublet (5.217 Å).

Here we present new atomic data for Si XII $1s^2nl$–$1snln'l'$ ($n' = 3$ and 4) satellites for both dielectronic and inner-shell excitation. Results are also given of an analysis of RESIK spectra during the decay stages of four long-duration flares in which fluxes of the Si XIII lines and Si XII satellites are derived. Synthetic spectra as a function of T_e based on our atomic data are in reasonable agreement with those observed by RESIK. We also studied the temperature dependence of the observed $n' = 3$ and 4 satellite–to–Si XIII line ratios with those calculated from our atomic data. An independent measure of T_e is provided by a number of line ratios in RESIK spectra, although these have not yet been quantified (see § 4). In the meantime, we used the less precise measure of T_e given by the ratio of the two broadband X-ray channels of the *Geostationary Operational Environmental Satellite* (*GOES*) ion chamber instruments. We found some disagreement between the theoretical curves and observed points having

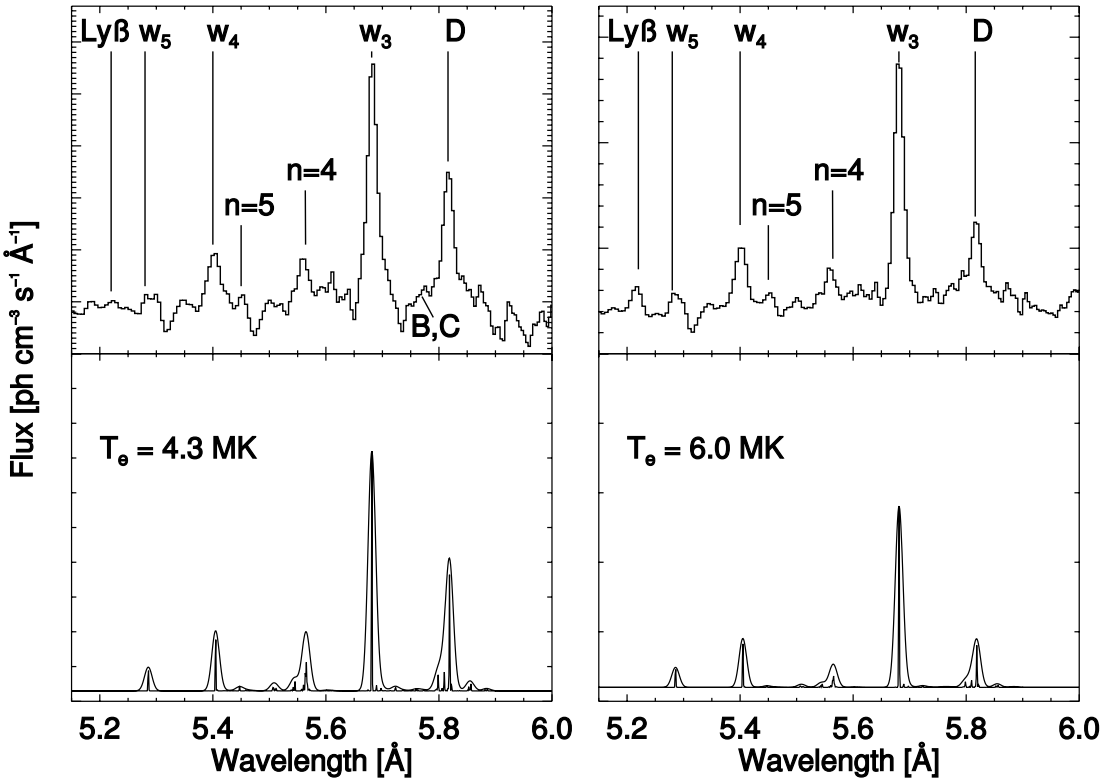

FIG. 1.—*Top panels*: RESIK spectra (absolute flux units) in the 5.15–6.0 Å range during the flare of 2002 July 26/27 at 27/10:03:32–10:21:56 UT (integrated over 1104 s; *left*) and 27/05:13:42–05:29:57 UT (976 s; *right*), showing the Si XIII w_3, w_4, and w_5 lines and nearby Si XII satellites. Components making up the $n = 3$ satellite feature are marked B, C, and D (see text). The Si XIV Lyβ line (marked) is at 5.22 Å. The temperatures determined from the ratio of emission in RESIK channel 1 to channel 4 were 4.3 and 6.0 MK. *Bottom panels*: Synthetic spectra with $T_e = 4.3$ MK (*left*) and 6.0 MK (*right*) and Gaussian line profiles with thermal Doppler profiles (ion temperatures assumed equal to T_e) and with FWHM = 15.7 mÅ to match the spectral resolution of RESIK channel 4. The Si XIII w_3, w_4, and w_5 lines are included, as are the Si XII $n = 4$ and 5 satellites.

high *GOES* temperatures, occurring in the early decay stages of each flare; for later times in the decay, when the *GOES* temperatures are lower, the disagreement is less pronounced. We attribute the disagreement to the nonisothermal nature of the flaring plasma, finding that there is some improvement in the agreement between observed and calculated ratios for simple model differential emission measures. Satellite lines due to Fe XXIV, similar to those discussed here for Si XII, occur at wavelengths of around 1.5 Å. In § 4, we point out the importance of these satellites, which are emitted by the hottest part of solar flare plasmas and by very hot nonsolar X-ray sources.

2. OBSERVATIONS AND ANALYSIS

The time evolution of the Si XIII $1s^2$–$1snp$ ($n \geq 3$) lines and nearby Si XII satellites is well illustrated with RESIK spectra during the decay phase of the 2002 July 26/27 flare, one of the four selected for analysis. Figure 1 (*top panels*) shows RESIK channel 4 spectra in the 5.15–6.0 Å region taken at two times during the flare decay, including the Si XIII w_3, w_4, and w_5 lines, as well as Si XII satellite features at 5.82 Å ($n = 3$), 5.56 Å ($n = 4$), and 5.44 Å ($n = 5$) (Sylwester et al. 2003). Emission detected by RESIK channel 4 is diffracted by quartz crystal (diffracting plane $10\bar{1}0$, $2d$ spacing 8.51 Å, and rocking curve FWHM = 0.62 mÅ). The spectral resolution (due primarily to detector position encoding uncertainty) has been empirically determined to be 15.7 mÅ (FWHM) from line widths during periods of flare decays and quiescent periods.

Using a careful instrument calibration established from prelaunch and postlaunch measurements (Sylwester et al. 2005), the temperatures characteristic of RESIK spectra can be determined from the ratio of the total emission in RESIK channel 1 (3.40–3.80 Å) and channel 4 (5.00–6.05 Å). For the two spectra in Figure 1, the estimated temperatures were 4.3 and 6.0 MK. The precision of these estimated temperatures varies according to the photon counts in channels 1 and 4; for spectra during the 2002 July 26/27 flare decay, the estimated uncertainties in the measured temperatures varied from ±1 MK to more than ±5 MK. Because of the sometimes large uncertainties in these temperature estimates, we sought alternative means of deriving plasma temperature. Several lines in the RESIK wavelength range are temperature dependent, although we have not yet derived theoretical ratios that take into account the spectral resolution of RESIK. Instead, we chose to use temperatures derived from the ratio of the two *GOES* channels. Use of temperatures from *GOES* is not ideal because of the broadband nature of the *GOES* channel. The channel ranges are approximately 0.5–4 and 1–8 Å and include both line and continuum emission. Derivation of temperatures from the *GOES* channel ratios has hitherto been based on the work of Thomas et al. (1985), who assumed a set of element abundances different from those now generally taken for the solar corona, in which elements of low first ionization potential are recognized as having enhanced abundances (Feldman & Laming 2000). The more recent algorithm of White et al. (2005) allows the use of coronal abundances and also includes atomic data from the CHIANTI code. We took *GOES* temperatures from the White et al. (2005) algorithm and assumed coronal abundances for the flare emission. Temperatures derived from the RESIK channel 1 to channel 4 emission ratios were found to be very similar to these *GOES* temperatures, as can be seen from Figure 2, based on measurements during the 2002 July 26/27 flare, which can therefore

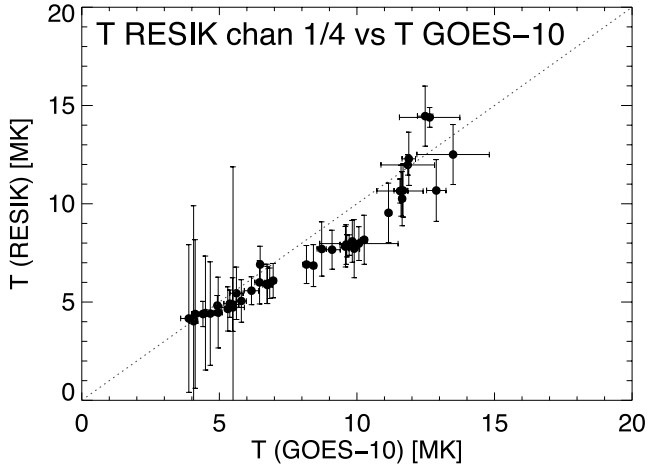

FIG. 2.—Temperatures T_e estimated from RESIK (ratio of channel 1 to channel 4 emission) plotted against those from *GOES* in intervals during the 2002 July 26/27 flare. [*See the electronic edition of the Journal for a color version of this figure*.]

be considered a validation of the RESIK ratio as a means of deriving temperatures for large enough photon counts in RESIK channels 1 and 4.

Details of the four long-duration flares selected for analysis, discussed previously by Phillips et al. (2003) for an element abundance study, are given in Table 1. All have significant Si XIII line emission for many hours, enabling repeated measurements of Si XII satellite and Si XIII line intensities. Over the course of each flare decay, RESIK spectra were accumulated in periods from 2.5 minutes (soon after flare maximum) to about 20 minutes (toward the end of the flare). Over these periods, the *GOES* flux and temperature showed no significant variation other than a slight decline. Times of small subsidiary events were excluded. Preflare emission was not subtracted from either the RESIK or *GOES* emission, as the final few RESIK spectra in each flare were very faint.

In Figure 3, the variations of line intensity in the 5.0–5.9 Å range over a 17.5 hr period during the 2002 July 26/27 flare are shown in a gray-scale representation (Fig. 3, *left*). The 29 times over which RESIK spectra were accumulated are stacked vertically (time increases upward) and show clearly how the Si XIII $1s^2$–$1s\,np$ line fluxes slowly decline while the fluxes of the Si XII satellites at 5.44, 5.56, and 5.82 Å increase. The *GOES* temperatures (Fig. 3, *right*), derived from the algorithm of White et al. (2005), decrease from 17 to 4 MK. These and other RESIK spectra were extracted using software written by one of us (J. S.; see Sylwester et al. 2005). In addition to giving absolute intensities from effective area data, the software subtracts a background due to crystal fluorescence and an instrumental fixed pattern structure and establishes a wavelength scale that takes into account nonlinearities in the position-sensitive detector and the source

TABLE 1
LONG-DURATION FLARES WITH RESIK OBSERVATIONS

Date (2002)	Time Range of RESIK Spectra (UT)	Time of Maximum *GOES* (1–8 Å) Flux	*GOES* Class
Apr 14.....	03:00–09:00	03:50	M1.3
Jul 11.....	15:45–20:00	14:50	M6
Jul 23.....	00:15–07:00	00:40	X5
Jul 26/27	26/21:23–27/15:00	26/21:00, 26/22:15	M9, M5

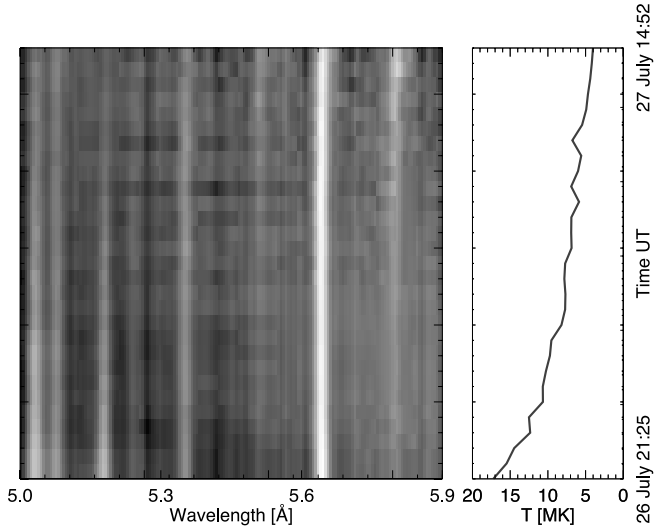

FIG. 3.—RESIK channel 4 spectra in the wavelength range 5.0–5.9 Å during the flare on 2002 July 26/27. The 29 spectra in gray-scale format (*left*) are stacked vertically (earliest times at the bottom, starting at 26/21:25 UT); they were integrated over periods from 2.5 minutes (near flare maximum) to 18 minutes (end of the flare). Bright emission lines are shown as vertical white streaks: they may be identified from Table 2. The increasing flux of the Si XII satellite feature at 5.82 Å and decreasing flux of the Si XIII 5.681 Å line as the flare emission and *GOES* temperature decline (*right*) are evident. [*See the electronic edition of the Journal for a color version of this figure*.]

offset relative to the disk center (along the instrument dispersion plane). A continuum is subtracted from each spectrum. The line fluxes discussed in § 4 were derived both from the excess emission above this continuum level at the expected line positions and from best-fit Gaussians to the line profiles. We found good agreement between the observed profiles and the Gaussian fits.

3. CALCULATED LINE SPECTRA

We calculated theoretical spectra using line excitation data from calculations presented here and from previous work. The Si XII

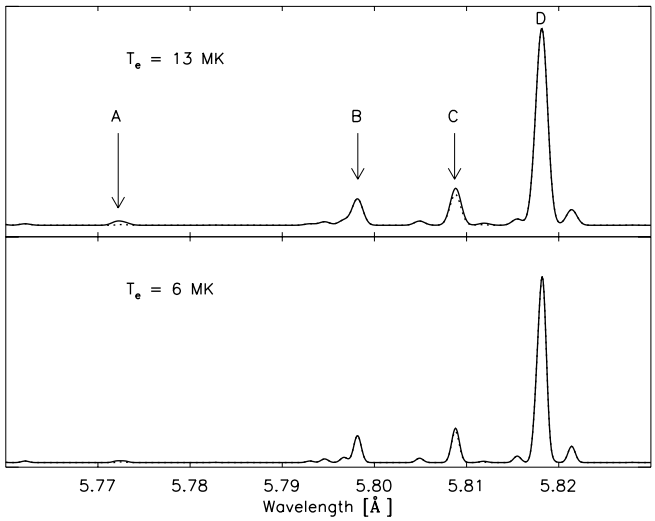

FIG. 4.—Synthesized spectra (5.76–5.83 Å) showing the Si XII satellite features A, B, C, and D (notation of Boiko et al. [1978] and Audebert et al. [1985]; see Table 2) for $T_e = 13$ and 6 MK. The spectra (*solid line*) show the total of dielectronic and inner-shell satellites; the dielectronic satellites alone (*dotted line*; most evident for feature C) are also shown. The line widths are for thermal Doppler broadening at 13 MK (FWHM 2.8 mÅ) and 6 MK (1.9 mÅ). At the resolution of RESIK (15.7 mÅ FWHM), the contribution of inner-shell satellites would be negligible.

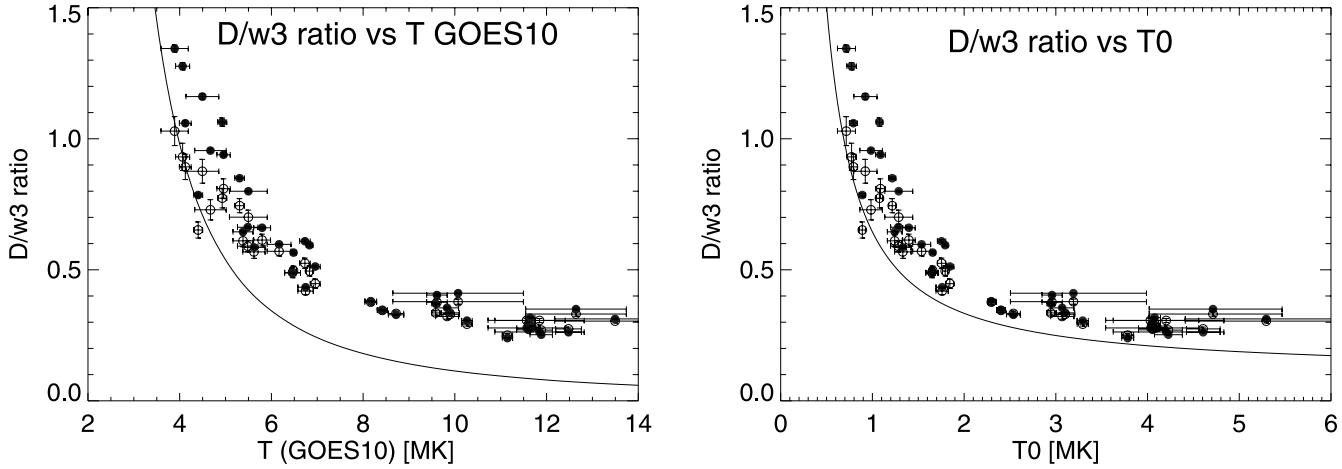

FIG. 5.—*Left*: Measured ratios of the principal satellite feature at 5.82 Å (marked D) to the Si XIII $w_3 + y_3$ line at 5.681 Å during the four flares of Table 1, plotted against T_e measured from *GOES* data. Filled circles denote line fluxes from Gaussian fits; open circles denote line fluxes from total flux above continuum level. The solid line is the calculated ratio. *Right*: Measured ratios plotted against T_0 for DEM $= \exp(-T_e/T_0)$. The solid line is the calculated curve.

satellite lines are formed principally by dielectronic recombination, but inner-shell excitation also occurs. The excitation has been described by Gabriel (1972) and Bely-Dubau et al. (1982), whose notation we follow. The photon flux at Earth (distance 1 AU) of a Si XII satellite line formed by dielectronic recombination of He-like Si ions, density $N_{\mathrm{Si\ XIII}}$ (cm^{-3}) in a coronal plasma, electron density N_e (cm^{-3}), temperature T_e, and volume V (cm^3), is

$$I_{\mathrm{sat}} = \frac{N_e N_{\mathrm{Si\ XIII}} V}{4\pi(\mathrm{AU})^2} \times \frac{2.06\times10^{-16}\ F_{\mathrm{sat}} \exp(-E_s/k_{\mathrm{B}}T_e)}{T_e^{3/2}}\ \text{photons cm}^{-2}\ \text{s}^{-1}, \quad (1)$$

where E_s is the excitation energy of the line's upper state above the ground state of the He-like ion, k_{B} is Boltzmann's constant, and F_{sat} is an intensity factor given by $F_{\mathrm{sat}} = A^r A^a/(A^a + \Sigma A^r)$. Here, A^r and A^a are transition probabilities from the satellite line's upper state by radiation and autoionization, respectively, and the summation represents radiative transition probabilities to all possible states below the satellite's upper state. Values of E_s for Si XII satellites are 120 ryd ($1s2l3l'$ upper levels) and 127 ryd ($1s2l4l'$ upper levels).

Values of A^r, A^a, F_{sat}, and wavelengths were calculated by one of us (J. D.) for Si XII satellites in the arrays $1s^2\,2l$–$1s\,2l\,nl'$, where $n = 3$ and 4. These calculations, which are an updated version of those by Audebert et al. (1985), were from the University College London (UCL) SUPERSTRUCTURE code (Eissner et al. 1974) and the AUTOLSJ code (Dubau & Loulergue 1982). All possible configurations $M\,1s^2\,nl$ and $1s\,nl\,n'l'$ with $n,\ n' = 2$, 3, and 4 M were included, giving a total of 54 configurations. The nl orbitals were calculated in scaled Thomas-Fermi-Dirac-Amaldi potentials, the scaling parameters being obtained by an energy minimization procedure: $\lambda_s = 3.318$, $\lambda_p = 2.048$, and $\lambda_d = \lambda_f = \lambda_g = 2.144$. The same l potentials were used to calculate the continuum states, $1s^2\,\epsilon l$, reached by autoionization. The transition probabilities were calculated using Fermi's golden rule. Relativistic effects were included by diagonalizing the Breit-Pauli Hamiltonian within bound configurations. Unresolved satellite intensities $1s^2\,nl$–$1s\,nl\,n'l'$, where $n = 3$ and 4 and $n' \geq n$ were also considered, but the contribution was found to be small due to

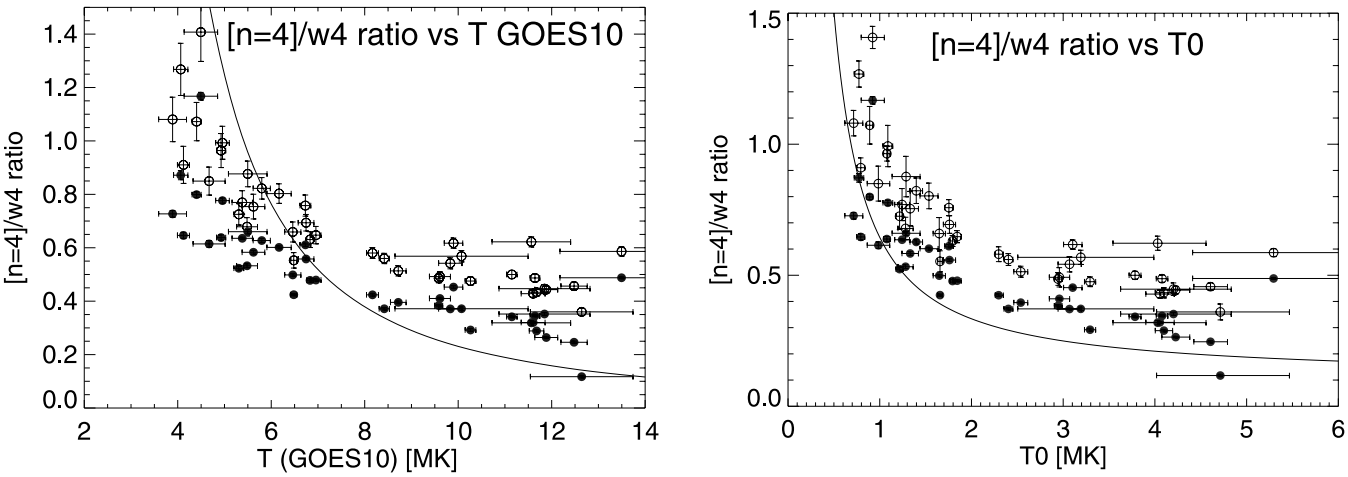

FIG. 6.—*Left*: Measured ratios of the principal Si XII satellite feature at 5.56 Å to the Si XIII $w_4 + y_4$ line at 5.405 Å during the four flares of Table 1, plotted against T_e measured from *GOES*. Filled circles denote line fluxes from Gaussian fits; open circles denote line fluxes from total flux above continuum level. The solid line is the calculated ratio. *Right*: Measured ratios plotted against T_0 for DEM $= \exp(-T_e/T_0)$. The solid line is the calculated curve.

TABLE 2

Si XIII Lines, Si XII Dielectronic Satellites, and Other Recognizable Lines in the 5.217–6.053 Å Region

Ion	Transition[a]	Wavelength[b] (Å)	Label[c]	B_r[d]	F_{sat}[d] (s^{-1})
Si XIV	$1s^2S_{1/2}$–$2p\ ^2P_{3/2}$	5.217	Lyβ_1	...	...
Si XIV	$1s^2S_{1/2}$–$2p\ ^2P_{1/2}$	5.218	Lyβ_2	...	...
Si XIII	$1s^2\ ^1S_0$–$1s6p\ ^1P_1$	5.223	Heϵ (w_6)	...	...
Si XIII	$1s^2\ ^1S_0$–$1s5p\ ^1P_1$	5.286	Heδ (w_5)	...	...
Si XIII	$1s^2\ ^1S_0$–$1s5p\ ^3P_1$	5.287	Heδ (y_5)	...	...
Si XIII	$1s2l$–$2l'3l''$	5.306–5.356	...	...	...
Si XIII	$1s^2\ ^1S_0$–$1s4p\ ^1P_1$	5.405	Heγ (w_4)	...	...
Si XIII	$1s^2\ ^1S_0$–$1s4p\ ^3P_1$	5.408	Heγ (y_4)	...	...
Si XII	$1s^2\ 2l$–$1s2l'5l''$	5.45	$n = 5$ sats	...	...
Si XII	$1s^22s\ ^2S_{1/2}$–$1s2p4p\ ^2P_{3/2}$	5.506	...	...	9.83E11
Si XII	$1s^22s\ ^2S_{1/2}$–$1s2p4d\ ^2D_{3/2}$	5.506	...	...	7.43E11
Si XII	$1s^22s\ ^2S_{1/2}$–$1s2s4p\ ^2P_{1/2}$	5.507	...	...	1.31E12
Si XII	$1s^22s\ ^2S_{1/2}$–$1s2p4s\ ^2P_{3/2}$	5.510	...	0.327	9.78E11
Si XII	$1s^22s\ ^2S_{1/2}$–$1s2p4s\ ^2P_{1/2}$	5.512	...	0.138	9.61E11
Si XII	$1s^22p\ ^2P_{1/2}$–$1s2p4p\ ^2D_{3/2}$	5.539	...	...	5.62E11
Si XII	$1s^22p\ ^2P_{3/2}$–$1s2p4p\ ^2D_{5/2}$	5.542	...	...	1.65E12
Si XII	$1s^22p\ ^2P_{3/2}$–$1s2p4p\ ^2D_{3/2}$	5.542	...	...	4.35E11
Si XII	$1s^22s\ ^2S_{1/2}$–$1s2s4p\ ^2P_{3/2}$	5.545	...	0.572	4.73E12
Si XII	$1s^22s\ ^2S_{1/2}$–$1s2s4p\ ^2P_{1/2}$	5.545	...	0.581	2.32E12
Si XII	$1s^22s\ ^2S_{1/2}$–$1s2s4p\ ^4P_{3/2}$	5.547	...	0.166	...
Si XII	$1s^22p\ ^2P_{1/2}$–$1s2p4p\ ^2S_{1/2}$	5.557	...	...	9.68E11
Si XII	$1s^22p\ ^2P_{3/2}$–$1s2p4p\ ^2S_{1/2}$	5.560	...	...	2.60E12
Si XII	$1s^22p\ ^2P_{1/2}$–$1s2p4p\ ^2D_{3/2}$	5.563	...	...	7.52E12
Si XII	$1s^22p\ ^2P_{3/2}$–$1s2p4f\ ^4G_{5/2}$	5.563	...	...	9.09E11
Si XII	$1s^22p\ ^2P_{3/2}$–$1s2p4p\ ^2D_{5/2}$	5.565	...	...	1.44E13
Si XII	$1s^22p\ ^2P_{3/2}$–$1s2p4f\ ^2F_{5/2}$	5.565	...	...	9.98E11
Si XII	$1s^22p\ ^2P_{3/2}$–$1s2p4f\ ^4F_{5/2}$	5.565	...	...	8.26E11
Si XII	$1s^22p\ ^2P_{1/2}$–$1s2p4p\ ^2P_{3/2}$	5.566	...	...	1.03E12
Si XII	$1s^22p\ ^2P_{3/2}$–$1s2p4p\ ^2D_{3/2}$	5.567	...	...	4.45E12
Si XII	$1s^22p\ ^2P_{3/2}$–$1s2p4p\ ^2P_{3/2}$	5.570	...	...	1.09E12
Al XIII	$1s\ ^2S_{1/2}$–$5p\ ^2P_{1/2,3/2}$	5.605	Lyδ	...	...
Si XIII	$1s^2\ ^1S_0$–$1s3p\ ^1P_1$	5.681	Heβ (w_3)	...	...
Si XIII	$1s^2\ ^1S_0$–$1s3p\ ^3P_1$	5.689	Heβ (y_3)	...	...
Si XII	$1s^24d\ ^2D_{3/2}$–$1s3p4d\ ^2F_{5/2}$	5.697	...	...	4.93E11
Si XII	$1s^24d\ ^2D_{5/2}$–$1s3p4d\ ^2F_{7/2}$	5.697	...	...	6.68E11
Si XII	$1s^23d\ ^2D_{5/2}$–$1s3p3d\ ^2F_{7/2}$	5.722	A	...	1.44E12
Si XII	$1s^23d\ ^2D_{3/2}$–$1s3p3d\ ^2F_{5/2}$	5.723	A	...	8.82E11
Al XIII	$1s\ ^2S_{1/2}$–$4p\ ^2P_{1/2,3/2}$	5.739	Lyγ	...	...
Si XII	$1s^22s\ ^2S_{1/2}$–$1s2p3s\ ^2P_{3/2}$ (M5)	5.759	...	...	5.22E11
Si XII	$1s^22s\ ^2S_{1/2}$–$1s2s3p\ ^2P_{3/2}$ (M4)	5.772	A	0.614	...
Si XII	$1s^22s\ ^2S_{1/2}$–$1s2s3p\ ^2P_{1/2}$ (K4)	5.773	...	0.684	...
Si XII	$1s^22p\ ^2P_{1/2}$–$1s2p3p\ ^2D_{3/2}$ (H10)	5.795	B	...	8.13E11
Si XII	$1s^22p\ ^2P_{3/2}$–$1s2p3p\ ^2P_{3/2}$	5.797	B	...	1.16E12
Si XII	$1s^22p\ ^2P_{3/2}$–$1s2p3p\ ^2D_{3/2}$	5.798	B	...	2.02E12
Si XII	$1s^22p\ ^2P_{3/2}$–$1s2p3p\ ^2D_{5/2}$	5.798	B	...	4.19E12
Si XII	$1s^22p\ ^2P_{1/2}$–$1s2p3p\ ^2S_{1/2}$	5.805	C	...	9.80E11
Si XII	$1s^22p\ ^2P_{3/2}$–$1s2p3p\ ^2S_{1/2}$	5.809	C	...	1.77E12
Si XII	$1s^22s\ ^2S_{1/2}$–$1s2s3p\ ^2P_{3/2}$ (M2)	5.809	C	0.669	3.84E12
Si XII	$1s^22s\ ^2S_{1/2}$–$1s2s3p\ ^2P_{1/2}$ (K2)	5.809	C	0.688	1.79E12
Si XII	$1s^22s\ ^2S_{1/2}$–$1s2s3p\ ^4P_{1/2}$ (K1)	5.812	...	0.571	...
Si XII	$1s^22s\ ^2S_{1/2}$–$1s2s3p\ ^4P_{3/2}$ (M1)	5.812	...	0.625	...
Si XII	$1s^22p\ ^2P_{1/2}$–$1s2s3d\ ^2D_{3/2}$	5.816	D	...	1.45E12
Si XII	$1s^22p\ ^2P_{3/2}$–$1s2p3p\ ^2D_{5/2}$	5.818	D	...	3.61E13
Si XII	$1s^22p\ ^2P_{1/2}$–$1s2p3p\ ^2D_{3/2}$	5.818	D	...	1.50E13
Si XII	$1s^22p\ ^2P_{3/2}$–$1s2p3p\ ^2D_{3/2}$	5.821	D	...	3.64E12
Si XII	$1s^22p\ ^2P_{1/2}$–$1s2s3d\ ^2D_{3/2}$	5.852	G	...	1.54E12
Si XII	$1s^22p\ ^2P_{3/2}$–$1s2s3d\ ^2D_{5/2}$	5.856	G	...	2.34E12
Si XII	$1s^22p\ ^2P_{1/2}$–$1s2s3s\ ^2S_{1/2}$	5.881	H	...	4.03E11
Si XII	$1s^22p\ ^2P_{3/2}$–$1s2s3s\ ^2S_{1/2}$	5.885	H	...	7.05E11
Al XIII	$1s^2S_{1/2}$–$3p\ ^2P_{1/2,3/2}$	6.053	Lyβ	...	...

[a] Si XII $n = 5$ satellites are identified from extrapolation (see text); Si XII $n = 3$ and 4 satellite transitions are from calculations given here; notation of Sampson et al. (1985) is included for some upper states of $n = 3$ satellites.

[b] Line wavelengths are from CHIANTI, except for Si XII satellites (calculations given here are for $n = 5$ satellites from RESIK observations).

[c] Notation of Boiko et al. (1978) is used for observed features corresponding to Si XII $n = 3$ satellites.

[d] From calculations given here; only dielectronic satellites with $F_{sat} > 4 \times 10^{11}$ s^{-1} are included.

additional autoionization decay channels to He-like excited states $1s2l$ and $1s3l$, which favor autoionization rather than radiation. It was also found that some $1s2l3l'$ states could cascade to $1s\,2l\,2l'$ states; excitation from these states therefore contributes to the intensities of satellites near the w line.

The Si XIII w_3 and w_4 lines are almost entirely formed by collisional excitation from the ground state, so their fluxes are approximately

$$I_{\mathrm{Si\ XIII}} = \frac{N_e N_{\mathrm{Si\ XIII}} V}{4\pi(\mathrm{AU})^2} \times \frac{8.63\times10^{-6}\ \Upsilon}{T_e^{1/2}} \exp\left(-\frac{E_0}{k_{\mathrm{B}}T_e}\right)\ \mathrm{photons\ cm^{-2}\ s^{-1}}, \quad (2)$$

where Υ is the temperature-averaged collision strength of the transition (energy E_0), a slowly varying function of T_e. Neglecting the weak y_3 and y_4 lines, the flux ratio of Si XII satellite to Si XIII parent line is thus

$$\frac{I_{\mathrm{sat}}}{I_{\mathrm{Si\ XIII}}} = 2.39\times10^{-11}\ \frac{F_{\mathrm{sat}}\exp[(E_0-E_s)/k_{\mathrm{B}}T_e]}{\Upsilon T_e}. \quad (3)$$

Values of E_0 for the w_3, w_4, and w_5 lines are 160.5, 168.7, and 172.5 ryd, respectively. Since the range of solar flare temperatures over which Si XII satellites have been observed in RESIK spectra is approximately 4–17 MK, the exponential factor in equation (3) varies from 1.3 to 4.1, so unlike the $n = 2$ satellites near the w line, a strictly T^{-1} dependence of $I_{\mathrm{sat}}/I_{\mathrm{Si\ XIII}}$ does not hold. Rather than use equation (2) for the w_3 and w_4 fluxes, we used $w_3 + y_3$ and $w_4 + y_4$ values from the CHIANTI atomic database and code (Dere et al. 1997) as a function of T_e.

We also considered inner-shell excitation of Li-like Si to produce satellites. In laser-produced plasmas with very high densities, excitation can proceed from the $1s^22s$ and $1s^22p$ states of Li-like Si. For densities $N_e \lesssim 5\times10^{17}$ cm^{-3}, i.e., including the relatively low densities of solar active regions and flares ($\sim10^{10}$–10^{11} cm^{-3}), excitation is only possible from $1s^22s$, and as a result the importance of inner-shell excitation is much reduced. It was nevertheless included in our calculations for $n = 3$ satellites. We used the collision strength data of Sampson et al. (1985) to derive temperature-averaged collision strengths Υ' of $1s^22s$–$1s2s3p$ inner-shell transitions. The line fluxes are given by

$$I'_{\mathrm{sat}} = \frac{N_e N_{\mathrm{Si\ XII}} V}{4\pi(\mathrm{AU})^2} \times B_r \frac{8.63\times10^{-6}\ \Upsilon'}{T_e^{1/2}} \exp\left(-\frac{E'_s}{k_{\mathrm{B}}T_e}\right)\ \mathrm{photons\ cm^{-2}\ s^{-1}} \quad (4)$$

for the excitation of $1s^22s$–$1s2l3l'$ transitions, where the branching ratio $B_r = A_r/(A_a + \Sigma A_r)$. The excitation energy E'_s is 156.8 ryd.

The flux ratio of an inner-shell Si XII satellite to Si XIII parent line is therefore

$$\frac{I'_{\mathrm{sat}}}{I_{\mathrm{Si\ XIII}}} = \frac{N_{\mathrm{Si\ XII}}}{N_{\mathrm{Si\ XIII}}} B_r \frac{\Upsilon'}{\Upsilon} \exp\left(\frac{E_0 - E'_s}{k_{\mathrm{B}}T_e}\right), \quad (5)$$

corresponding to equation (3).

The calculated fluxes and wavelengths of the Si XII satellites, together with CHIANTI values for the Si XIII lines, were used as input to an IDL routine written to synthesize spectra with input values of T_e. Ionization fractions of Mazzotta et al. (1998; needed for inclusion of inner-shell excited satellites) were used. Gaussian shapes for the line profiles were assumed, with widths chosen by the user. Synthetic spectra using this routine are shown in the bottom panels of Figure 1, with temperatures equal to those derived from the RESIK channel 1 to channel 4 ratio. The line profiles are given by both the RESIK instrumental resolution and thermal Doppler broadening (with ion temperature equal to T_e). Line broadening due to plasma broadening, of slight significance near the onset of each flare, is neglected in this figure. In Figure 4 the very small contribution made by inner-shell satellites in the $1s^22s$–$1s2s3p$ array is shown by synthetic spectra in the 5.76–5.83 Å range for thermal Doppler-broadened lines; the contribution is clearly negligible for solar flare spectra observed with RESIK. The synthetic spectral routine was also used to find the theoretical variation with T_e of the ratios of satellite features at 5.82 and 5.56 Å, $I(5.82)/I(w_3)$, and $I(5.56)/I(w_4)$. Satellites in the spectral ranges 5.78–5.83 and 5.53–5.575 Å were included. These ratios as a function of T_e are shown as the solid lines in Figures 5 (*left*) and 6 (*left*), respectively.

Table 2 is a list of all significant lines in the range 5.217–6.053 Å. It includes Si XIII lines, all the Si XII dielectronically formed $n = 3$ and 4 satellites from our calculations having $F_{\mathrm{sat}} > 4\times10^{11}$ s^{-1} (about 1% of the maximum value), and Si XII satellites formed by inner-shell excitation. Observed lines of H-like Si (Si XIV) and Al (Al XIII) in this range are also included. The Si XII $n = 3$, 4, and 5 satellites cluster together to form observed line features. The $n = 3$ satellite features are well resolved in laser-produced plasma spectra; see Boiko et al. (1978) and Audebert et al. (1985), whose letter (A–H) notation for them is given in Table 2 and Figure 4. In RESIK flare spectra, the single prominent feature at 5.82 Å is identified with D, with features B and C forming a short-wavelength tail to D (see Fig. 1). Lines with corresponding transitions form the Si XII $n = 4$ satellite line feature at 5.56 Å. Although we did not calculate atomic data for the Si XII $n = 5$ satellites, we identified the feature at 5.45 Å in RESIK spectra with a group of $n = 5$ satellites from the intensity variation with T_e and the wavelength difference from the w_5 line. Other Si XII line wavelengths in Table 2 are those calculated here; they are between 1 and 2 mÅ larger than the wavelengths given by Audebert et al. (1985). Values of B_r for the inner-shell satellites are also given in the table.

4. RESULTS AND CONCLUSIONS

The comparisons of RESIK flare spectra with those synthesized from atomic data at temperatures indicated by RESIK channel ratios (Fig. 1) seem to indicate that the atomic theory describing the satellite–to–parent line intensity ratio is reliable. However, a more detailed analysis shows that there are significant departures of observed intensities from theory. For each of the flares listed in Table 1, flux measurements were made of the $n = 3$ and 4 satellite features and the Si XIII w_3 and w_4 lines. The measurements were made by subtracting the continuum from RESIK channel 4 spectra and fitting Gaussian profiles to the line emission. Estimates were also made from the excess fluxes above the continuum level at the line positions without fitting profiles.

Both sets of measurements were taken over short time intervals during which the measured *GOES* temperature changed only slightly. Figure 5 (*left*) shows the theoretical ratio of the $n = 3$ satellite feature D (5.82 Å) to the Si XIII w_3 line as a function of T_e, together with observed ratios by the two line flux measuring

techniques. For ratios late in the flare decay, when the *GOES* T_e was relatively small ($\sim$4 MK; no preflare background subtracted), there is reasonably good agreement between the observed points and the curve. But ratios measured at or shortly after the maximum of each flare are 2 or 3 times that predicted by theory. For measured ratios of the Si XII $n = 4$ satellite feature (5.56 Å) to the Si XIII w_4 line (Fig. 6, *left*), the ratios late in each flare decay are below the theoretical curve, while those shortly after flare maximum are, like the $n = 3$ satellites, well above the theoretical curve.

Some of the discrepancy between theoretical and observed ratios may be attributed to the limitations of deriving temperatures from *GOES* ratios, as indicated in § 2. However, it is also likely that the nonisothermal nature of the flaring plasma makes some contribution. Thus, an emission measure distribution extending over the temperature range 4–14 MK would, if decreasing with T_e, explain the discrepancy. To see this, we take a differential emission measure (DEM) having the form of a monotonically decreasing function of T_e, e.g., DEM = const $\times \exp(-T_e/T_0)$ or const $\times T^{-\alpha}$, where T_0 and α are constants, with no upper or lower temperature limits. At flare maximum or shortly after, the DEM shape is likely to be only slowly decreasing with T_e (i.e., T_0 large or α small), reflecting the great complexity of these events. Indeed, *Transition Region and Coronal Explorer* (*TRACE*) extreme ultraviolet and *RHESSI* images of the four flares of Table 1 show loops with temperatures ranging from 1 to 20 MK. Since the Si XII satellites have $G(T_e)$ or contribution functions that peak at slightly lower temperatures than the Si XIII lines, the ratio of satellite to parent line will be larger than for an equivalent isothermal value of T_e. Later in the flare decay, the DEM dependence on T_e is likely to be much more steeply falling (i.e., T_0 small or α large), and the emission of either the Si XII satellites or Si XIII lines covers only a small temperature range. This explains the observation by Phillips et al. (2005) of Ca XIX and S XV temperatures converging to similar values during the late stages of long-duration flares seen by *Yohkoh*.

The effect that differential emission measure makes on these line ratios is deferred to a later, more detailed study (J. Sylwester et al. 2006, in preparation). Meanwhile, we illustrate how the line ratios are a function of T_0 for the case where the differential emission measure takes the functional form DEM = const $\times \exp(-T/T_0)$, with no lower or upper temperature limits. The satellite or He-like ion line fluxes $I_{\rm DEM}$ are given by

$$I_{\rm DEM} = \text{const} \times \int G(T_e) \exp(-T_e/T_0)\, dT_e, \qquad (6)$$

where $G(T_e)$ is the contribution function, i.e., the function that includes all the atomic factors and ion fractions in equations (1), (2), and (4). To determine T_0, we use the ratio $R_{\rm DEM}$ of the emission (F_l and F_s) in the long-wavelength (1–8 Å) and short-wavelength (0.5–4 Å) channels of *GOES*, given by

$$R_{\rm DEM} = \frac{\int F_s \exp(-T_e/T_0) dT_e}{\int F_l \exp(-T_e/T_0) dT_e}. \qquad (7)$$

Figure 5 (*right*) shows the theoretical ratio of the Si XII $n = 3$ (D) satellites to the Si XIII $w_3 + y_3$ lines (from eq. [6]) and observed ratios plotted against T_0, derived from *GOES* ratios. Note that the range of T_0 values is much smaller than the equivalent range of T_e values and that the points agree better with the theoretical curve. Figure 6 (*right*) is the equivalent plot for the ratio of Si XII $n = 4$ satellites to the Si XIII $w_4 + y_4$ lines. Again, the theoretical curve is in better agreement than for the isothermal case. The reason for the remaining nonagreement is likely to be the assumed form for the DEM. Other DEM forms are currently being tested (J. Sylwester et al. 2006, in preparation).

We may conclude that the satellite to line ratios discussed here are sensitive indicators of electron temperature T_e for isothermal plasmas or of the temperature dependence of differential emission measures when these are assumed to have a simple analytical form. They may also be used as input into differential emission measure codes such as DEMON (Sylwester et al. 1980) and PINTofALE (Kashyap & Drake 2000).

The equivalent of the Si XII satellites discussed here emitted by the Li-like stages of other elements should also be of interest, particularly in the case of Fe. Fe XXV lines with transitions $1s^2$–$1s\,np$ occur at 1.573 Å ($n = 3$), 1.495 Å ($n = 4$), and 1.461 Å ($n = 5$). Fe XXIV dielectronic satellite features occur on the long-wavelength side of these lines, at 1.593, 1.516, and 1.460 Å, respectively. Their intensities relative to their parent lines have the same kind of T_e dependence as for the Si lines, giving a useful temperature diagnostic for the hottest part of the solar flare plasma. Although these lines have not yet been seen with crystal-spectrometer resolution, broadband instruments such as *RHESSI* (cooled germanium detectors: Lin et al. 2002) and the Si PIN detector on the *Near Earth Asteroid Rendezvous* (*NEAR*) spacecraft (Trombka et al. 2001) have observed these lines as a single unresolved feature at $\sim$1.55 Å (8.0 keV). The spectral resolution of *RHESSI* is at best 0.98 keV (FWHM; Smith et al. 2002), and $\sim$0.6 keV (FWHM) for the Si PIN detector. The dependence on T_e of this feature's intensity relative to the nearby continuum is a sensitive one, enabling flare plasmas to be diagnosed (Phillips 2004). An instrument with much better resolution, e.g., $\sim$6 eV at 6 keV, such as the now-defunct XRS microcalorimeter instrument on the *Suzaku* spacecraft (Fujita et al. 2005), could resolve all the satellite structure. For solar-type sources, such as stellar flares and other plasmas for which there is coronal ionization and excitation equilibrium, the Fe XXIV $n = 3$ and 4 satellite line–to–parent line ratios, as illustrated for Si in this work, should be useful diagnostics of T_e (if isothermal) or differential emission measure (if nonisothermal).

The RESIK project (PI: J. Sylwester) is a common project between the Space Research Centre (Poland) and the Naval Research Laboratory (US), Mullard Space Science Laboratory, and Rutherford Appleton Laboratory (UK). J. S. and B. S. acknowledge support from grant 1 P03D 017 29 of the Polish Committee for Scientific Research. K. J. H. P. acknowledges support from a National Research Council Senior Research Associateship award. CHIANTI is a collaborative project involving the Naval Research Laboratory, Rutherford Appleton Laboratory (UK), and the Universities of Florence (Italy) and Cambridge (UK).

REFERENCES

Audebert, P., Geindre, J. P., Gauthier, J. C., Chenais-Popovics, C., Cornille, M., Dubau, J., & Faucher, P. 1985, Phys. Rev. A, 32, 3120
Bely-Dubau, F., Dubau, J., Faucher, P., & Gabriel, A. H. 1982, MNRAS, 198, 239
Boiko, V. A., Pikuz, S. A., Safronova, U. I., & Faenov, A. Y. 1978, MNRAS, 185, 789
Dere, K. P., Landi, E., Mason, H. E., Monsignori Fossi, B. C., & Young, P. R. 1997, A&AS, 125, 149
Doschek, G. A. 1972, Space Sci. Rev., 13, 765
Dubau, J., & Loulergue, M. 1982, J. Phys. B, 15, 1007
Eissner, W., Jones, M., & Nussbaumer, H. 1974, Comput. Phys. Commun., 8, 270

Feldman, U., Doschek, G. A., Nagel, D. J., Cowan, R. D., & Whitlock, R. R. 1974, ApJ, 192, 213
Feldman, U., & Laming, M. 2000, Phys. Scr., 61, 222
Fujita, Y., Matsumoto, T., Wada, K., & Furusho, T. 2005, ApJ, 619, L139
Gabriel, A. H. 1972, MNRAS, 160, 99
Kashyap, V., & Drake, J. J. 2000, Bull. Astron. Soc. India, 28, 475
Lin, R. P., et al. 2002, Sol. Phys., 210, 3
Mazzotta, P., Mazzitelli, G., Colafrancesco, S., & Vittorio, N. 1998, A&AS, 133, 403
Neupert, W. M. 1971, Sol. Phys., 18, 474
Phillips, K. J. H. 2004, ApJ, 605, 921
Phillips, K. J. H., Feldman, U., & Harra, L. K. 2005, ApJ, 634, 641
Phillips, K. J. H., Sylwester, J., Sylwester, B., & Landi, E. 2003, ApJ, 589, L113
Sampson, D. H., Goett, S. J., Petrou, G. V., Zhang, H., & Clark, R. E. H. 1985, At. Data Nucl. Data Tables, 32, 343
Smith, D. M., et al. 2002, Sol. Phys., 210, 33
Sylwester, J., Schrijver, J., & Mewe, R. 1980, Sol. Phys., 67, 285
Sylwester, J., Sylwester, B., Culhane, J. L., Doschek, G. A., Oraevsky, V. N., & Phillips, K. J. H. 2003, in Proc. ISCS Symp. (ESA SP-535; Noordwijk: ESA), 733
Sylwester, J., et al. 2005, Sol. Phys. 226, 45
Thomas, R. J., Starr, R., & Crannell, C.-J. 1985, Sol. Phys., 95, 323
Trombka, J. I., et al. 2001, Meteoritics Planet. Sci., 36, 1605
Walker, A. B. C., & Rugge, H. R. 1971, ApJ, 164, 181
White, S. M., Thomas, R. J., & Schwartz, R. A. 2005, Sol. Phys., 227, 231